Mesoscale Kinetic Monte Carlo Simulations of Molecular Resists: The Effect on PAG Homogeneity on Resolution, LER, and Sensitivity

Richard A. Lawson[a] and Clifford L. Henderson[a*]

[a]School of Chemical & Biomolecular Engineering, Georgia Institute of Technology
Atlanta, GA 30332-0100

* Corresponding Author: cliff.henderson@chbe.gatech.edu

ABSTRACT

A two-dimensional kinetic Monte Carlo mesoscale model of molecular resists was developed to probe the effects of photoacid (PAG) homogeneity, specifically PAG aggregation behavior, on the resolution, sensitivity, and line edge roughness performance of resists. The model reproduces many pattern defects that are commonly found experimentally simply by increasing the amount of PAG aggregation. The sensitivity of resists was found to change with increasing PAG aggregation in resists with low photoacid diffusivity, but remain near constant for resists with high photoacid diffusivity. Likewise, LER was found to increase with increasing PAG aggregation in resists with low photoacid diffusivity, but appears to be weakly dependent on PAG aggregation when the resist has photoacids with high diffusivity. Increasing PAG aggregation limits the absolute resolution of a resist because there exists a trade-off between the ability of photoacid diffusion to smooth out the inhomogeneity due to PAG aggregation and the blurring of the patterned feature that reduces resolution. Even very low levels of PAG aggregation appear to greatly limit the potential of a resist for sub-30 nm resolution patterning, but increased PAG loading appears to provide a way to mitigate this problem and allow for improved absolute resolution even in the presence of aggregation.

Keywords: chemically amplified photoresist, mesoscale model, stochastic model, resolution, sensitivity, line edge roughness, photoacid generator, homogeneity, aggregation

1. INTRODUCTION

Line edge roughness (LER) is an increasing concern for the continued reduction in critical feature sizes for integrated circuits and other microelectronic devices because the size scale of LER is rapidly becoming a significant portion of the total feature size.[1] While there has been much effort to model chemically amplified resist (CAR) physics that may induce LER such as shot noise effects[2] and photoacid diffusion and reaction[3], little work has been done to model material homogeneity effects that may contribute to LER, especially photoacid generator (PAG) homogeneity.

While PAGs are essential to the proper function of modern CARs, it has been observed that the most commonly used ionic types of these small molecule additives can tend to aggregate and phase separate from the resist resin to some degree, regardless of whether the resin is a molecular glass or polymer.[4-5] This segregation creates a number of problems that ultimately can induce LER.[6] Since typical PAGs can behave as dissolution inhibitors, if they aggregate they can suppress or prevent dissolution at their random cluster locations. Similarly, an aggregate of irradiated PAGs can cause random locations of higher photoacid concentration that can lead to regions of higher than expected resist dissolution rate. Such localized inhomogeneity in dissolution behavior could obviously lead to roughness behavior in a resist. Beyond LER, PAG aggregation can even have significant effects on resolution and sensitivity for many smaller features as feature sizes begin to approach that of potential PAG aggregate sizes.

Continuum based models have long been used to simulate photoresist behavior, and this approach allows for fast simulation of resist performance and can model global inhomogeneities such as concentration gradients due to exposure effects (e.g. standing waves, absorption, etc.). Unfortunately, the utility of continuum models is limited for modeling LER, localized material homogeneity effects such as PAG aggregation, and the stochastic behavior of individual events like PAG decomposition and acid diffusion. The length scales of interest are rapidly approaching the size of individual

Advances in Resist Materials and Processing Technology XXVI, edited by Clifford L. Henderson,
Proc. of SPIE Vol. 7273, 727341 · © 2009 SPIE · CCC code: 0277-786X/09/$18 · doi: 10.1117/12.814447

Downloaded From: http://spiedigitallibrary.org/ on 12/17/2012 Terms of Use: http://spiedl.org/terms

resist component molecules, and thus the resist behavior becomes strongly influenced by such stochastic effects. Several groups have investigated the use of mesoscale stochastic modeling to investigate the properties of materials at these length scales,[7-11] but they have not thoroughly examined the effects PAG homogeneity, especially PAG aggregation, on the performance of resists. To fully probe these issues, a full kinetic Monte Carlo mesoscale simulation of molecular resists has been developed to probe the effect of resist composition, processing parameters, and PAG aggregation on the resolution, sensitivity, and LER of CARs, extending our earlier work in the area that only examined the effect on LER.[12]

2. MODEL DESCRIPTION

2.1 Model Description

The model is based on a two-dimensional lattice with 1 nm by 1 nm cells. The total simulation domain is 150 by 150 cells. A molecular resist containing three protecting groups or a PAG is placed inside each cell. The simulation study that was used in this case required that all three protecting groups must be removed to render the resist molecule soluble. The simulation set-up is graphically illustrated in Figure 1. The lattice sizing of 1 nm by 1 nm was chosen because it was a good approximation of the size a representative molecular resist[13] and it provided a molecular density that is consistent with the experimental mass density of bulk samples of this resist.

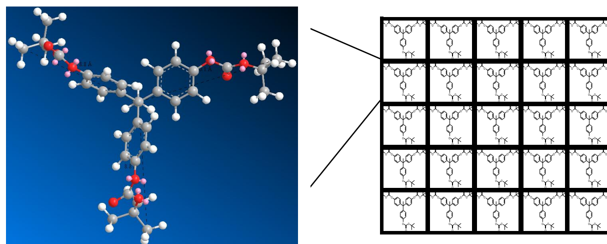

Figure 1. Schematic illustrating the lattice model setup used in this work.

Ideal aerial image profiles consisting of a step function were used for exposure simulation. Photoacid generation was executed using the Dill C equation to determine the probability of an acid being generated for a given exposure dose. For this study, a C parameter of 0.03 cm^2/mJ was used in the Dill C equation. This Dill C corresponds to 95% of all PAGs being converted to photoacids at a dose of 100 mJ/cm^2. During the PEB step, the photoacids random walk from lattice site to lattice site and carry out deprotection and the specifics of how this is done are described later. After the simulation is completed, resist molecules that meet the solubility criteria (fully deprotected) are removed and insoluble molecules are left intact to create the final imaged feature.

The reaction-diffusion of photoacids during the PEB step is carried out using the kinetic Monte Carlo method by considering the relative rates of photoacid diffusion and the deprotection reaction. This is slightly different than an earlier version of this model that assumed very fast reaction and only considered the rate of diffusion.[14] The rate of photoacid diffusion is proportional to the acid diffusion coefficient D. The rate of deprotection is the deprotection rate constant, k, times the number of protecting groups at the lattice site where an acid resides. The total summation of rates for the system, R_N, is the summation of the diffusion rate and deprotection rate of every acid in the lattice. A uniform random number between 0 and 1 is multiplied by R_N to determine which event occurs and which acid carries out that event. By this method, the event with the fastest rate is the statistically most likely to occur. When k is much greater than D, then acids will effectively completely deprotect a site when they land on it before diffusing to another site. When D is greater than k, acids will diffuse to many different sites before removing any protecting groups. Simulation time during each cycle is updated by the same method as Gillespie[15] until it reaches 60 seconds, thus representing a normal 60 second post-exposure bake (PEB) time.

The main parameter used to describe the level of PAG aggregation in this work is referred to as the PAG aggregate size. For each simulation, the PAG loading and PAG aggregate size is specified. The PAG loading determines the total

Downloaded From: http://spiedigitallibrary.org/ on 12/17/2012 Terms of Use: http://spiedl.org/terms

number of PAGs that are present in the system as a function of the total fraction of lattice sites (e.g. a PAG loading of 0.05 (5%) implies that 5% of the total lattice sites contain a PAG). PAG aggregate size determines the average number of PAGs that make up an aggregate. To maintain an equivalent total number of PAGs for different aggregate sizes, the PAG loading is divided by the aggregate size to determine the number of "seed PAGs" for each simulation. The aggregates are formed by selecting a seed PAG and randomly adding PAGs in sites directly adjacent to it until the correct number of PAGs form each aggregate as determined by the aggregate size. In the case of a PAG aggregate size of 1, the number of seed PAGs is equivalent to the total number of PAGs and no aggregates are intentionally formed, although some aggregates may still form due to the stochastic nature of the PAG placement into lattice. Likewise, for a PAG aggregate size of 25, the number of seed PAGs is $1/25^{th}$ the number of total PAGs. Figure 2 graphically shows the effect of increasing PAG aggregate size on the initial distribution of PAGs in the lattice.

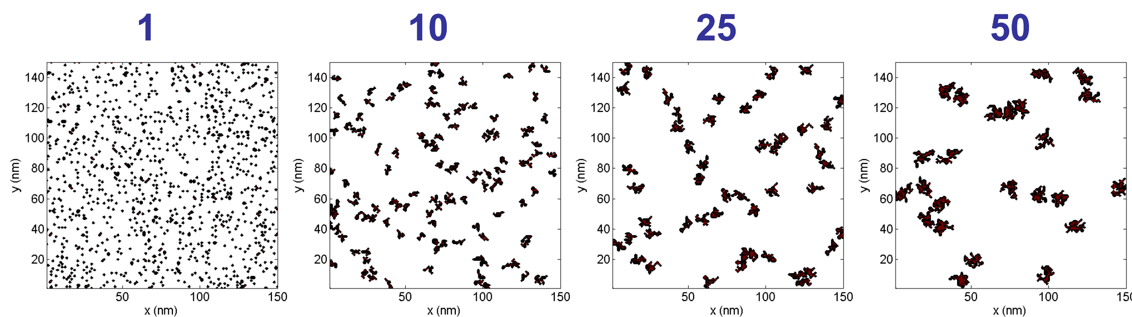

Figure 2. Effect of increasing PAG aggregate size on PAG distribution for a total PAG loading of 5%. PAG aggregate size is the number above the plots.

Since the model is a two dimensional representation of three dimensional physics, certain differences arise that must be accounted for properly. Because diffusion into the third dimension is not possible in the two dimensional lattice, the average time for an acid jump during diffusion must be modified such that the mean squared displacement for an acid is the same as it would be in three dimensions. In other words, the effective deprotection circle of the acid should be equivalent to the two dimensional projection of the deprotection sphere that would occur in a three dimensional lattice. This is accounted for when describing the rate of diffusion in this model, and the mean squared displacement of individual acids scale correctly with D.

Likewise, LER determined from the two dimensional model as reported in this paper is expected to be different from the LER observed in real three dimensional resist structures since LER is normally determined using a top-down SEM image. So in real three dimensional resist structures the LER that is commonly reported is actually the edge roughness of the projected line edge as viewed from above. Thus, the LER values from the model reported in this paper are higher than those generally reported from experimental measurements due to the fact that the model used in this work looks essentially only at one horizontal slide in a resist film. There is no chance for different resist feature slices with various large roughness features at their line edge to overlap when viewed from top down and appear as a smoother projected line edge. Despite this, the two-dimensional model accurately captures the physical response of the system to changes in variables such as acid diffusion coefficient, and it is simply the case that the LER reported will be some multiple larger than for a thick resist film. In essence, the simulation represents an infinitely thin resist film which would indeed be expected to show larger roughness than thicker resist films as confirmed by a number of recently reported studies of the effect of resist film thickness on LER. Although the LER values are large, changes in system parameters that change LER will have the same effect (i.e. if LER in the model gets larger, then LER in thick resist film structures should also get larger experimentally). In general, the two-dimensional model accurately provides information about the system response in terms of changes in LER, just with larger LER values than would be experimentally determined.

Downloaded From: http://spiedigitallibrary.org/ on 12/17/2012 Terms of Use: http://spiedl.org/terms

3. RESULTS AND DISCUSSION

3.1 Effect of PAG Aggregation on Resolved Patterns

While the quantitative results provide useful information regarding the effect of PAG aggregation on resolution, LER, etc., it is also useful to graphically examine the effect of aggregation on a patterned feature. Figure 3 shows the combined effects of aggregation on initial PAG distribution, final photoacid distribution after the PEB, and the final developed feature shape for several PAG aggregate sizes in the case of low photoacid diffusivity. It shows how PAG aggregation leads to clustered areas of low and high acid concentration which then lead to several different types of commonly observed defects. While these patterns are only for a single simulation run each, they provide a representation of how the quantitative results that are described later come about. When the level of aggregation is low, the pattern forms with good continuity and exhibits moderate-to-low LER. As the amount of aggregation increases (10), the pattern is still resolved, but small defects begin to appear and the LER increases. As the aggregation increases even more, the patterns begin to show major defects. For aggregate sizes of 25, the pattern mostly resolves, but has major defects such as the so-called "mouse bite" defect along the line edge. Even larger levels of aggregation lead to patterning failure where significant portions of the pattern do not resolve and bridging defects begin to dominate the pattern.

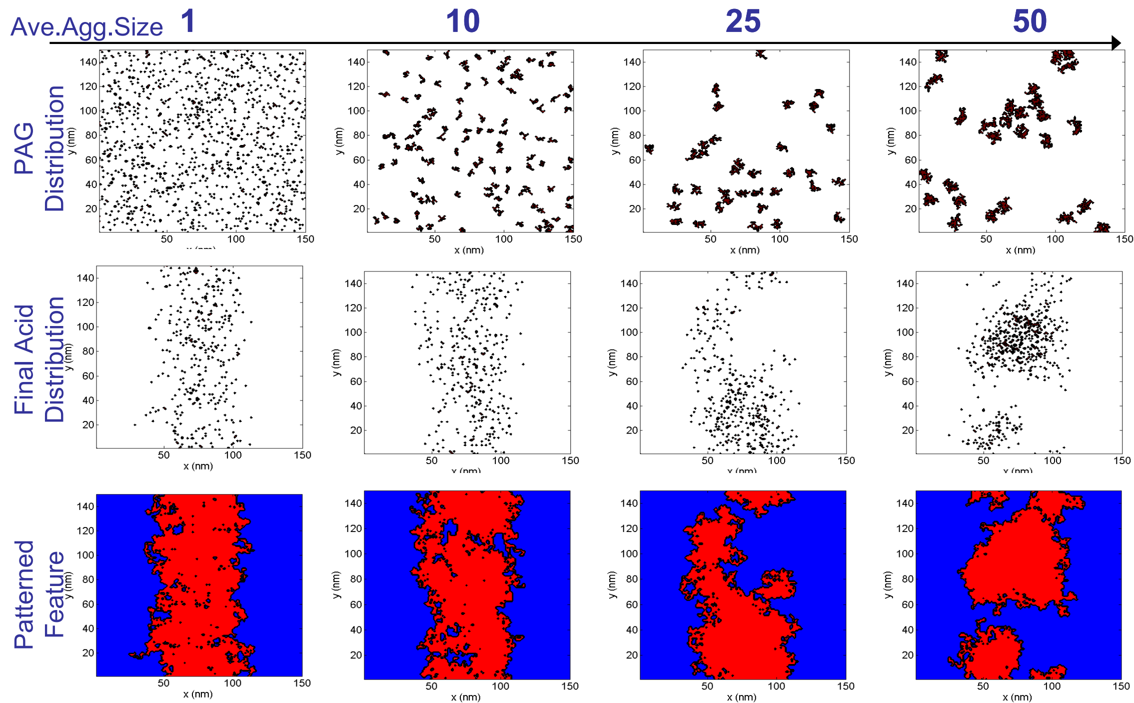

Figure 3. Graphical representation of how PAG aggregation can produce many commonly observed pattern defects.

3.2 Effect of PAG Aggregation on Resolution, Line Edge Roughness, and Sensitivity

There are three main metrics that are used when comparing the patterning capability of resist materials: resolution, line edge roughness, and sensitivity (i.e. now commonly referred to as "RLS"). The effect of PAG aggregation on each of these parameters was examined. Many of the model results regarding RLS can be explained using the concept of deprotection spheres, and so a short discussion of the concept will be given here. After an individual photoacid is created, it diffuses (i.e. random walks) and reacts with protecting groups in its vicinity during the PEB to effectively create a somewhat spherical region of deprotected resist.[16] For a stochastic system such as the one reported here, each individual deprotected region will not be a true sphere due to the random nature of a stochastic simulation, but the concept of a sphere is still useful in describing the results. The size of this deprotection sphere is dependent on the time

Downloaded From: http://spiedigitallibrary.org/ on 12/17/2012 Terms of Use: http://spiedl.org/terms

of the PEB, the diffusion coefficient *D* of the photoacid, and the deprotection rate constant *k*. Increasing each of these parameters effectively increases the size of the deprotection sphere, as demonstrated in Figure 4. A feature can typically only be patterned if the deprotection spheres of the acids in the exposed area overlap sufficiently to render that area soluble.

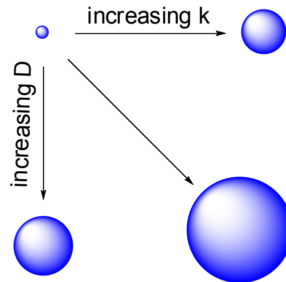

Figure 4. Graphical representation of how the deprotection sphere of a photoacid increases with increasing *D* and *k*.

While sensitivity generally describes the amount of energy required to pattern a resist, it may have many meanings depending on what specifically is patterned. The sensitivity derived in our simulation is essentially the dose-to-size, the dose required to pattern a feature to the nominally correct size. Dose-to-size changes due to a combination of things including the aerial image log slope, the resist contrast, the diffusivity of the photoacid, the deprotection reaction rate constant, PAG aggregation and segregation, etc. For the purposes of our study, we examined PAG aggregation, photoacid diffusivity, and deprotection rate constant *k*. Given these three parameters, there are a large number of possible combinations of conditions that could be examined. Figure 5 provides representative examples for the major effects that are seen through changes in these variables. Figure 5a shows the effect of PAG aggregate size in the case of low photoacid diffusivity (D = 0.18 nm^2/s) with a number of different deprotection reaction rate constants. Figure 5b shows the same results for the case of higher photoacid diffusivity (D = 1.8 nm^2/s).

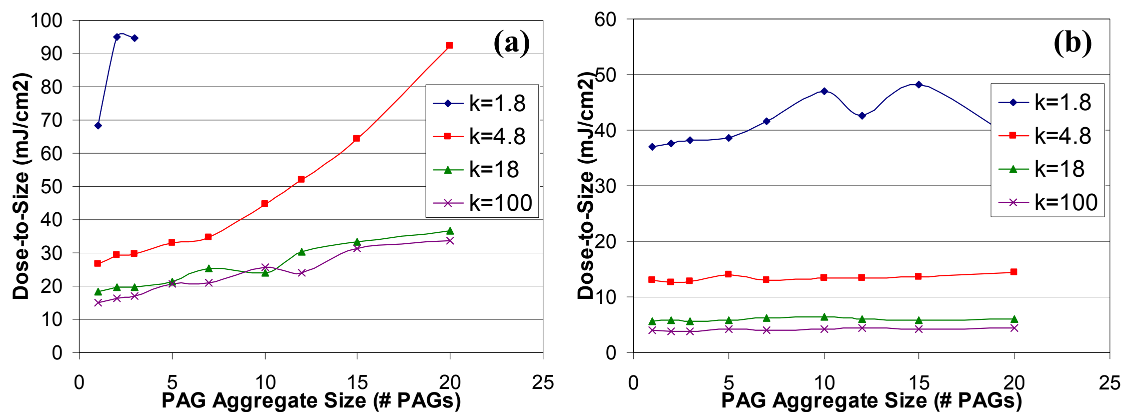

Figure 5. Effect of PAG aggregate size on dose-to-size for: (a) low acid diffusivity, (b) high acid diffusivity

When photoacid diffusivity is low (Figure 5a), the dose-to-size increases as the amount of PAG aggregation increases. This result can be explained easily using the deprotection sphere concept. When the amount of PAG aggregation increases, the distribution of acids within the exposed area is less homogeneous. Since the acids are initially clustered together instead of spread out, more acids must be generated in order for their individual deprotection spheres to overlap sufficiently to completely clear the feature. This likewise explains the effect of reaction rate constant. For low *k* values, the deprotection spheres are smaller, so higher dose is required to generate enough spheres to clear the patterned area. For this same reason, the curve for low *k* stops at aggregate sizes of 3-5 because at larger aggregate sizes, there is

Downloaded From: http://spiedigitallibrary.org/ on 12/17/2012 Terms of Use: http://spiedl.org/terms

insufficient overlap even when all the acids are generated to clear the pattern. As *k* increases, the dose-to-size decreases because the deprotection spheres are larger and fewer are required to sufficiently overlap, while at high *k* there is little change as *k* increases because the deprotection is diffusion controlled since the deprotection reaction is so much faster than the diffusion jumps.

For the case of high photoacid diffusivity (Figure 5b), the dose-to-size stays relatively constant as aggregate size increases. Since the diffusivity is high, the deprotection spheres are sufficiently large that they overlap even for large amounts of aggregation; the photoacid diffusion acts to smooth out the initially inhomogeneous distribution of acids. This is similar to what was seen in previous studies that showed that diffusion could smooth out inhomogeneity that was due to the standing wave phenomenon in resists.[17] When *k* increases, the dose-to-size decreases because the deprotection spheres get larger until the deprotection again becomes diffusion controlled.

LER is likewise an important parameter that characterizes the quality of the resist performance. While LER can be evaluated for a number of conditions, it is most useful to characterize the LER of the resist at the dose-to-size (E_{size}); even if the LER of a material is good, if the desired feature can't be printed, the low LER is of little use. Figure 6a shows the effect of PAG aggregation on LER for low photoacid diffusivity (D = 0.18 nm^2/s), while Figure 6b shows the same result for high photoacid diffusivity (D = 1.8 nm^2/s). In the case of low acid diffusivity, LER increases linearly with increasing aggregate size, and changing k only has a small effect on LER. While the deprotection spheres can overlap sufficiently to clear the nominal pattern size, they do not significantly smooth out the initial inhomogeneity in PAG loading. Since the clusters of PAGs are not evenly distributed, there are areas of high acid density and areas of low acid density; this leads to areas of the resist that clear outside the nominal line edge and areas that do not clear all the way to the line edge. The average line edge is correct, but the large variations in the local line edge lead to increased LER. PAG aggregation is the dominant factor in controlling LER in this case.

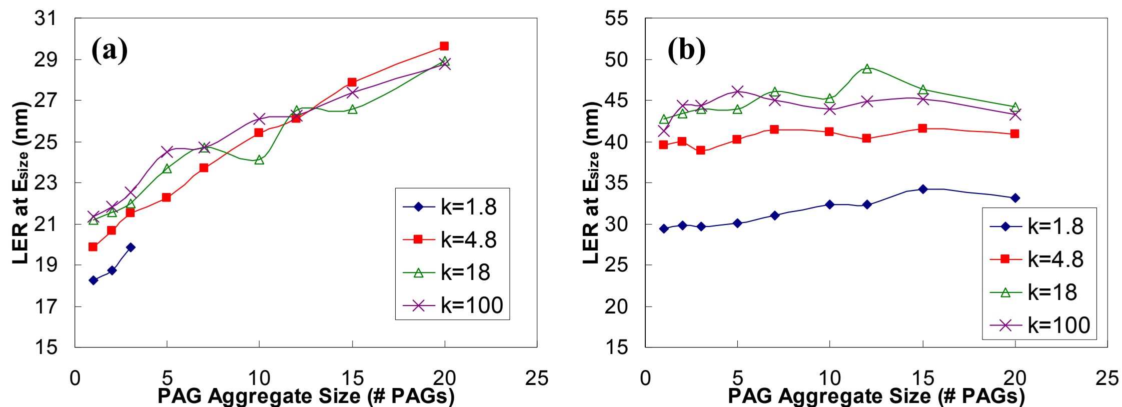

Figure 6. Effect of PAG aggregate size on LER for: (a) low acid diffusivity, (b) high acid diffusivity

In the case of high photoacid diffusivity (Figure 6b), the LER remains nearly constant as PAG aggregation increases. This result is similar to the result for dose-to-size at high diffusivity, and in this case the diffusion of the photoacid acts to smooth out the inhomogeneity of the initial acid distribution. Since the inhomogeneity due to PAG aggregation is greatly reduced, it no longer is the controlling factor in LER formation in the resist, and now the diffusion of photoacids outside of the exposed area acts as the dominant factor in causing LER. While the deprotection sphere concept is useful for describing many of the results, individual photoacids do not diffuse spherically, their walk is random and this result reinforces this fact. The diffusion outside of the exposed region is due to the random walk nature of diffusion; since there is a distribution of diffusion lengths, some acids diffuse far outside of exposed region. This is also seen in the effect of *k* on LER. At low values for *k*, the LER is much lower than at high values of *k* because even if isolated acids diffuse far outside the exposed regions, they cannot carry out enough deprotection reactions to make these outer regions soluble. Although higher photoacid diffusivity allows for smoothing out the initial PAG aggregation, there is a trade-off between the smoothing effect on LER and diffusion significantly outside of the nominally patterned region.

The LER and sensitivity results can also be better understood by graphically comparing the behavior of the two cases of low and high photoacid diffusivity. Figure 7a and Figure 7b show the PAG distribution and final acid distribution,

Downloaded From: http://spiedigitallibrary.org/ on 12/17/2012 Terms of Use: http://spiedl.org/terms

respectively, for low acid diffusivity (D = 0.18 nm^2/s) and Figure 7c and Figure 7d show the PAG distribution and final acid distribution, respectively, for high acid diffusivity (D = 1.8 nm^2/s). In the case of low acid diffusivity in Figures 7a and 7b, there is visibly little smoothing away from the PAG aggregates, but likewise minimal diffusion of photoacids outside of the exposed region (i.e. the exposed region lies between x coordinates 50 and 100 nm in these simulations). The most obvious flaw in the line-edge in Figure 7b is in the location of initially low PAG concentration region in the upper right portion of the exposed region. Comparing the left and right line edges in Figure 7b, the left edge has low LER except near the top of the feature, while the right edge has significant roughness due to the aggregation. Although this is obviously an extreme case of inhomogeneity, it demonstrates the dominant mechanisms in the case of low diffusivity. In the case of high acid diffusivity (i.e. Figure 7c and Figure 7d), the inhomogeneity due to PAG aggregation is smoothed out to the point that it is hard even to determine where the regions of low and high PAG concentration were when looking only at the final acid distribution in Figure 7d. The roughness of the line edge is no longer due to the PAG distribution, but due to the acids which have visibly diffused outside of the exposed region (i.e. those acids in Figure 7d lying to the left of the x=50 nm coordinate or to the right of the x=100 nm coordinate).

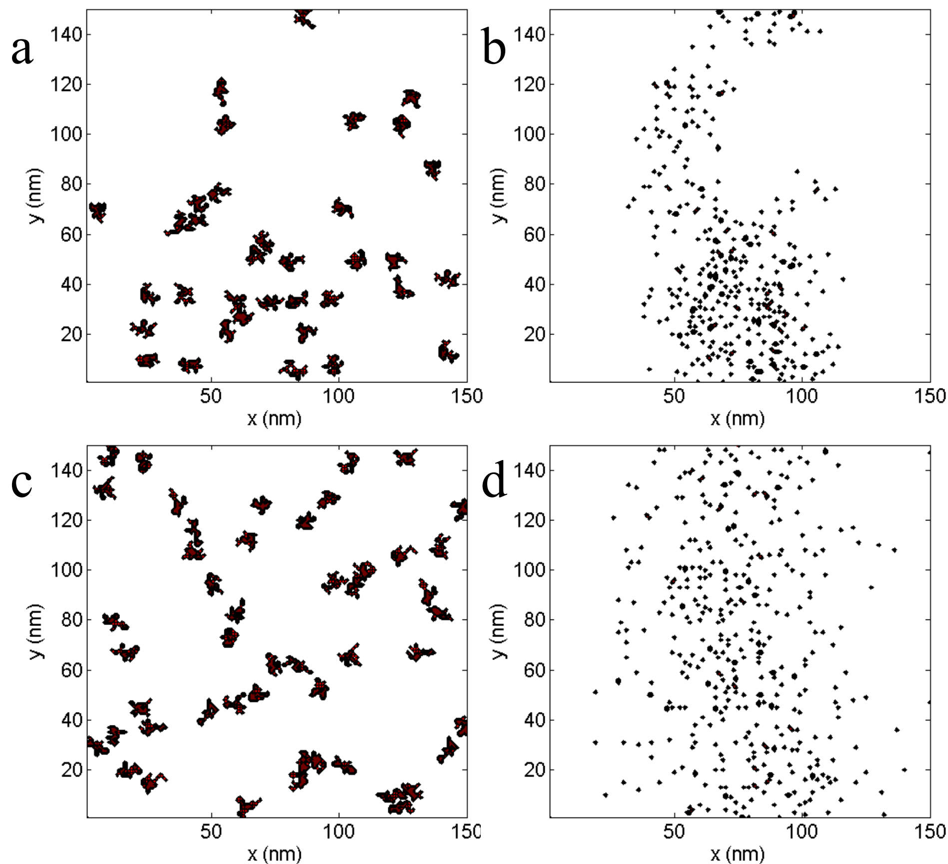

Figure 7. Graphical representation of the smoothing effect of photoacid diffusion, (a) PAG distribution for an aggregate size of 25, (b) the final photoacid distribution of (a) after diffusion for low diffusivity, (c) different PAG distribution for an aggregate size of 25, (d) the final photoacid distribution (c) after diffusion for high diffusivity.

The effect of PAG aggregate size on resolution is best examined by determining the minimum resolution that can be obtained for a given aggregate size, or alternatively, what is the maximum aggregate size that will print a specific resolution. The later comparison will be the used to examine the effect on resolution because it basically sets a limit for what level of aggregation is tolerable at each desired resolution. To determine the maximum aggregate size allowable, the simulation was run for a large number of reaction rate constants and photoacid diffusivities to cover the full range of potential processing conditions and material properties; the maximum aggregate size that would still resolve a feature with the correct CD (based on the average CD of 50 simulation runs) was taken to be the maximum for that feature size.

Downloaded From: http://spiedigitallibrary.org/ on 12/17/2012 Terms of Use: http://spiedl.org/terms

Figure 8 shows the results for a PAG loading of 5% as was used to generate the previous results. As one might expect, for large feature sizes, the maximum allowable aggregate size is reasonably large. This is because the acid diffusion lengths required to smooth out this level of inhomogeneity are still small relative to the feature size and so higher levels of photoacid diffusion allow for larger aggregate sizes. As the feature sizes shrink, the allowable aggregate size also shrinks because diffusion lengths must also shrink in order to maintain CD. Since the diffusion lengths must be smaller, the average spacing between PAG aggregates must shrink. Although higher diffusivity allows for smoothing out the initial PAG aggregates, there is a trade-off between the smoothing effect and the blurring of the feature. Ultimately, some aggregates require such a high diffusivity that the desired CD can never be patterned due to photoacid diffusion blur. This becomes especially important for sub 30 nm feature sizes, as the allowable amount of PAG aggregation reduces to no more than a few PAGs for a standard PAG loading of 5%.

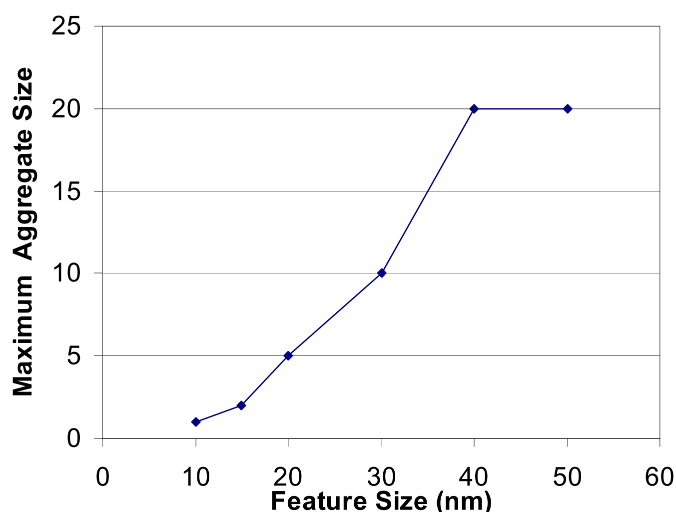

Figure 8. Maximum PAG aggregate size that can be tolerated to successfully print the desired feature size for a PAG loading of 5%.

Given that the standard PAG loading puts such restrictions on the allowable aggregate size, alternative resist "formulations" were examined using the simulation by changing the PAG loading and determining the maximum aggregate size allowable for obtaining features of different sizes. The results for this study are shown in Figure 9. As the PAG loading increases, the allowable PAG aggregate size tends to increase for all resolutions. This is because there are more total PAGs in the film, and if the number of PAGs in each individual aggregate are the same then the higher PAG loadings will have a larger number of aggregates. This reduces the spacing between aggregates, meaning that shorter diffusion lengths are required to smooth out the inhomogeneity due to the PAG aggregates. While there are only moderate gains for slightly increased PAG loading, increasing the PAG loading to 25% greatly improves the ability to print patterns down to sub-20 nm. This PAG loading could likely be achieved with minimal modification to standard resists. In the limit of ultra-high PAG loading, the density of PAG molecules is so high that they cannot effectively aggregate because if every resist molecule is a PAG, the resist is molecularly homogeneous. While this level of PAG loading may seem unfeasible to experimentally obtain, it has been shown to be possible given the correct resist designs.[18] This ultra-high PAG loading would potentially allow for patterning of any feature size regardless of PAG aggregation.

Downloaded From: http://spiedigitallibrary.org/ on 12/17/2012 Terms of Use: http://spiedl.org/terms

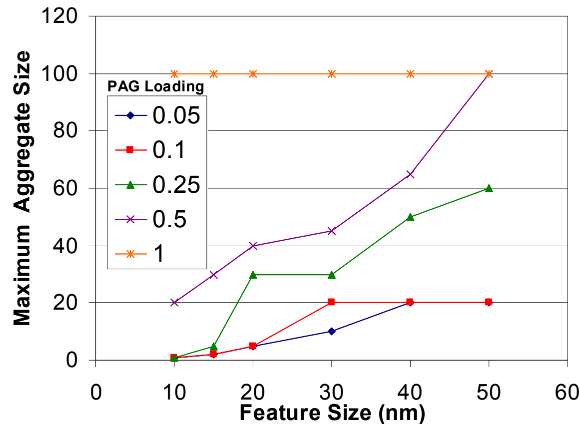

Figure 9. Maximum PAG aggregate size that can be tolerated and successfully print the desired feature size for different PAG loadings.

4. CONCLUSIONS

A two-dimensional kinetic Monte Carlo mesoscale model of molecular resists was developed to probe the effects of PAG homogeneity, specifically PAG aggregation behavior, on the resolution, sensitivity, and line edge roughness performance of resists. By increasing the amount of PAG aggregation, the model was able to reproduce many common experimentally encountered defects such as line bridging. The required dose-to-size for resists with relatively low photoacid diffusivity was found to increase with increasing PAG aggregation, while higher diffusivity photoacids show little change with increasing aggregation because the photoacids can diffuse sufficiently far to smooth out the initial inhomogeneities in acid distribution. Similarly to dose-to-size, the LER of a resist with low diffusivity photoacids increases with increasing PAG aggregation because the acids do not diffuse far enough to smooth out the initial photoacid inhomogeneity. Resists with higher photoacid diffusivity show little change in LER with increasing PAG aggregation because the acid diffusion smoothes out the initial inhomogeneity. For most conventional PAG loadings, increasing PAG aggregation leads to loss of absolute resolution, and this becomes especially problematic for patterning sub-30 nm features. The loss of resolution is due to the fact that the smaller features greatly restrict the allowable diffusion length of the photoacids, and there is a trade-off between the smoothing effect that corrects for PAG inhomogeneity and blurring of the feature that reduces resolution. Simulations also suggest that higher PAG loadings can potentially solve this problem and allow for photoresists with better ultimate resolution.

ACKNOWLEDGEMENTS

The authors would like to gratefully acknowledge Intel Corporation for funding this research and would also like to thank Dr. Jeanette Roberts, Dr. Steve Putna, Dr. Todd Younkin, and Dr. Wang Yueh at Intel for helpful discussions related to this work.

REFERENCES

1. M. Chandhok, Proc. SPIE **6519**, 6519A (2007).
2. R. L. Brainard, P. Trefonas, J. H. Lammers, et al., Proc. SPIE*,* **5374**, 74, (2004).
3. K. A. Lavery, V. M. Prabhu, E. K. Lin, et al., Appl. Phys. Lett, **92**, 064106, (2008).
4. J. T. Woodward, J. Hwang, V. M. Prabhu, et al., AIP Conf. Proc., **931**, 413, (2007).

Downloaded From: http://spiedigitallibrary.org/ on 12/17/2012 Terms of Use: http://spiedl.org/terms

5. E. L. Jablonski, V. M. Prabhu, S. Sambasivan, et al., Proc. SPIE, **5376**, 302, (2004).
6. T. Hirayama, D. Shiono, et al., Proc. SPIE, **5753**, 738, (2005).
7. D. Drygiannakis, G. P. Patsis, N. Tsikrikas et al., Microelectron. Eng., **85**, 949, (2008).
8. D. Drygiannakis, G. P. Patsis, I. Raptis et al., Microelectron. Eng., **84**, 1062 (2007).
9. G. M. Schmid, S. D. Burns, M. D. Stewart et al., Proc. SPIE, **4690**, 381-390 (2002).
10. G. M. Schmid, M. D. Stewart, S. D. Burns et al., J. Electrochem. Soc., **151**, G155, (2004).
11. N. Tsikrikas, D. Drygiannakis, G. P. Patsis et al., Jpn. J. Appl. Phys., Part 1, **46**, 6191, (2007).
12. R.A. Lawson, C.L. Henderson, Microelectron. Eng. (2009), doi:10.1016/j.mee.2008.12.042
13. R. A. Lawson, C. T. Lee, C. L. Henderson et al., J. of Vac. Sci. Technol. B, **25**, 2140 (2007).
14. R. A. Lawson, C. T. Lee, W. Yueh et al., Proc. SPIE, **6923**, 69230Q (2008).
15. D.T. Gillespie, J. Phys. Chem **81**, 2340 (1977)
16. S. Kang, B. D. Vogt, W. L. Wu et al., Macromolecules, **40**, 1497, (2007).
17. P. Trefonas III, B.K. Daniels, M.J. Effer, et al., Proc. SPIE, **920**, 203 (1988).
18. R. A. Lawson, C.-T. Lee, W. Yueh et al., Proc. SPIE, **6923**, 69230K (2008).

Downloaded From: http://spiedigitallibrary.org/ on 12/17/2012 Terms of Use: http://spiedl.org/terms